Carbohydrate Polymers 117 (2015) 988–995

Contents lists available at ScienceDirect

Carbohydrate Polymers

journal homepage: www.elsevier.com/locate/carbpol

Effect of structure and viscosity of the components on some properties of starch-rich hybrid blends

Willian H. Ferreira, Marwin M.I.B. Carmo, Ana Lúcia N. Silva, Cristina T. Andrade*

Instituto de Macromoléculas Professora Eloisa Mano, Universidade Federal do Rio de Janeiro, Centro de Tecnologia, Bloco J, PO Box 68525, 21941-598 Rio de Janeiro, RJ, Brazil

ARTICLE INFO

Article history:
Received 19 August 2014
Received in revised form 11 October 2014
Accepted 13 October 2014
Available online 28 October 2014

Keywords:
Thermoplastic starch
Poly(lactic acid)
Hybrid blends
Extrusion
Injection molding

Chemical compounds studied in this article:
Starch (PubChem CID: 24836924)
Poly(lactic acid) (not found)

ABSTRACT

Glycerol-plasticized cornstarch and poly(lactic acid) (PLA) were melt-blended alone and at a constant 70:30 (m/m) composition, in the present of an organoclay. The effect of increasing contents of the organoclay on extruded and compression-molded samples was evaluated by X-ray diffraction (XRD), capillary rheometry, thermogravimetric analysis (TGA), scanning electron microscopy (SEM), and tensile tests. XRD and shear viscosity results obtained for the hybrid components (TPS/organoclay and PLA/organoclay) were correlated with the hybrid blends properties. XRD and TGA results suggested that the organoclay was similarly dispersed within both phases. SEM images revealed improved adhesion between the phases. Shear viscosities results indicated improved compatibilization as the organoclay content was increased. Some of the extruded materials were also submitted to injection molding, and characterized by SEM and by tensile tests. For the extruded and compression-molded samples, improved mechanical properties were obtained for the samples with higher contents of the organoclay. For the injection-molded samples, the mechanical properties seemed to be dependent on the organoclay dispersion.

1. Introduction

Poly(lactic acid) (PLA) and starch are considered promising biobased materials to substitute traditional petroleum-based polymers. PLA is a biocompatible and bioresorbable polyester, with mechanical properties similar to poly(ethylene terephathalate) and polystyrene. Until the late 1980s, the application of PLA was mainly focused on the biomedical field, as a biomaterial for hard tissue replacement or in controlled drug delivery systems. However, the high hydrophobic character and, consequently, slow hydrolytic degradation rate, was appointed as a disadvantage to some applications (Luckachan & Pillai, 2011).

The interest in starch-based materials has grown because of their relatively low cost, renewability and biodegradability in most environments. Starch consists of two polysaccharides, amylose and amylopectin, both formed by D-glucose repeating units. The semicrystalline structure of starch granules is destroyed by thermomecanical treatment in the presence of suitable plasticizers, leading to thermoplastic starch (TPS). However, the sensitivity of TPS to ambient humidity practically invalidates its commercial use. Because of this drawback, the development of TPS blends and composites has been investigated. Blending TPS with PLA would maintain the biodegradability of the resulting materials, and might improve their properties.

It was postulated that blend properties are determined by the structural characteristics of each component and the phase morphology developed during melt processing. The final morphology is controlled by blend composition, rheological properties of the components, interfacial tension and viscosity ratio between the components, and processing conditions (Sundararaj & Macosko, 1995; Wu, 1987).

Much effort has been made to develop TPS/PLA blends. The low interfacial adhesion between hydrophilic starch and hydrophobic PLA has been recognized as the major problem to be overcome. To promote the compatibility of these materials, maleic anhydride was added in one or two stages (Huneault & Li, 2007; Wang, Yu, & Ma, 2007; Zhang & Sun, 2004). On the other hand, some authors followed three strategies; *in situ* formation of urethane linkages, *in situ* coupling of starch and PLA with peroxide, and addition of previously formed PLA-grafted amylose as compatibilizing agent (Schwach, Six, & Avérous, 2008). Improvements in mechanical properties were obtained for the blends with PLA in excess, substituting PLA for maleated PLA or

* Corresponding author. Tel.: +55 21 2562 7208; fax: +55 21 2270 1317.
E-mail addresses: ctandrade@ima.ufrj.br, cristina.andrade@pq.cnpq.br (C.T. Andrade).

http://dx.doi.org/10.1016/j.carbpol.2014.10.018
0144-8617/

by using PLA-grafted amylose. Additionally, to prepare PLA/TPS blends, other authors used maleated PLA and sodium montmorillonite (MMT) at 2% content, as a compatibilizing and a reinforcing agent, respectively. Before processing, MMT was added either to a starch water-glycerol suspension or to PLA. For the blends with 60% TPS, the location of MMT at the TPS phase led to higher modulus and strength enhancement (Arroyo, Huneault, Favis, & Bureau, 2010). In another report, small amounts of MMT (0.5 and 1% based on potato starch dry mass) were also incorporated to a TPS/PLA blend at 60/40 composition, in a multi-stage process, which consisted of potato starch gelatinization, ultrasonic dispersion of MMT in water and melt mixing at 185 °C for 10 min. Reduction in water absorption and improvements in mechanical and dynamic-mechanical properties were observed (Ayana, Suin, & Khatua, 2014).

Similarly to the stabilization of foams and oil-in-water emulsions (Horozov, 2008; Hunter, Pugh, Franks, & Jameson, 2008), nanoparticles may inhibit coalescence of dispersed phase droplets in immiscible polymer blends, mainly when located at their interface. However, the location of nanoparticles is dictated by thermodynamic interactions, kinetic and viscosity effects (Feng, Chan, & Li, 2003; Fenouillot, Cassagnau, & Majesté, 2009). Also, as postulated previously by these authors, the stabilization of morphology is a requisite to maintain constant properties (Fenouillot et al., 2009).

In this work, glycerol-plasticized cornstarch was melt-blended with PLA at a 70:30 constant composition without the addition of a compatibilizing agent, under one-step extrusion processing. Differently from the works cited before (Arroyo et al., 2010; Ayana et al., 2014), an organically-modified clay was also incorporated with increasing contents (1.0 to 10.0 mass%) to the polymeric components. Both polymeric components were also extruded and compression-molded alone and in the presence of the organoclay at the same contents, and were characterized by X-ray diffraction and capillary rheometry. The objectives of these experiments were to investigate the organoclay dispersion within TPS and PLA matrices, determine changes in flow behavior resulting from the filler addition, and mainly investigate the influence of these features on some properties of the resulting hybrid blends. For this, TPS/PLA/organoclay blended materials were also characterized by thermogravimetric analysis. The mechanical and morphological properties were investigated for the extruded and compression-molded samples and for some of the extruded materials, which were injection-molded.

2. Experimental

2.1. Materials

Regular cornstarch (CS) was supplied by Ingredion Brasil—Ingredientes Industriais Ltda. (São Paulo, SP, Brazil). According to the producer, this material is composed of 26–30 mass% amylose and 74–70 mass% amylopectin, with less than 0.5 mass% gluten. The gravimetric method was used to determine the humidity content (12 mass%). Analytical grade glycerol was purchased from Vetec Química Fina (Rio de Janeiro, RJ, Brazil) and was used as received. Poly(lactic acid) (PLA, NatureWorks LLC, Ingeo 2002D, with melt flow index of 4–8 g/10 min at 190 °C/2.16 kg) was supplied as pellets by Cargill Agrícola S.A. (São Paulo, SP, Brazil). This PLA sample was previously characterized by gel permeation chromatography in chloroform, and the results reported as M_n = 121,100 and M_w = 197,000 (Souza, Dahmouche, Andrade, & Dias, 2013). PLA pellets were cryogenically ground into powder to ensure better mixing with the other components. Cloisite® 30B (C30B), a montmorillonite modified with dihydroxyethyl alkyl methylammonium ions, was supplied by Southern Clay Products (Gonzales, TX, USA), and was used as received.

2.2. Preparation of samples

The mixture of CS and glycerol, added at 25 mass% based on starch dry mass, was homogenized in a conventional mixer (Ika Works, Wilmington, NC, USA) for 30 min, and maintained in tightly sealed polyethylene bags for 48 h at 4 °C before processing to obtain TPS. Glycerol-plasticized CS and PLA were mixed separately with C30B at 1.0, 2.5, 5.0, 7.5 and 10.0 mass% contents to obtain TPS/C30B and PLA/C30B materials. To obtain TPS/PLA/C30B hybrid blends, glycerol-plasticized CS and PLA were homogenized at a constant 70:30 (m/m) ratio and the organoclay was added at 1.0, 2.5, 5.0, 7.5 and 10.0 mass% contents, over the total mass of the polymers.

2.3. Extrusion and compression molding

Extrusion processings were carried out in a Coperion ZSK 18 (Werner & Pfleiderer, Stuttgart, Germany) co-rotating twin-screw extruder, with a L/D ratio of 40 and seven heating zones. For glycerol-plasticized CS with various amounts of C30B, the seven heating zones were maintained at 110, 110, 115, 115, 115, 110, 110 °C, and the screw speed was set at 120 rpm. For PLA and the blends (obtained by one-step extrusion processings) with varying amounts of C30B, the seven heating zones were maintained at 160, 160, 165, 165, 165, 160, 160 °C, and the screw speed was set at 120 rpm. The PLA/C30B materials showed free-flowing behavior and were cooled in a water bath after extrusion. All extruded materials were pelletized and compression-molded by heating at different temperatures (TPS at 120 °C, PLA and the hybrid blends at 165 °C) under 68.9 MPa for 10 min, and cooling for 5 min in a cold press. The resulting sheets, with 12 cm × 10 cm × 2 cm dimensions, were used for the materials characterization.

2.4. X-ray diffraction (XRD)

The samples were analyzed with a Ultima IV diffractometer (Rigaku Corporation) in the angular region 0.9 to 10° (2θ) at a 0.01° s^{-1} rate, in reflection mode. The Cu$K\alpha$1 radiation with wavelength of 1.542 Å was generated at 40 kV and 20 mA. The d-values were calculated by the Bragg's law (Eq. (1)).

$$n\lambda = 2\,d\,\mathrm{sen}\,\theta \tag{1}$$

where n is an integer, λ is the wavelength of incident wave (1.5418 Å), d is the spacing between any two atomic planes in the crystal lattice, and θ is the angle of reflection.

2.5. Capillary viscosity measurements

A Göttffert capillary rheometer model Rheograph 25 (Buchen, Germany), equipped with a round-hole capillar of D = 1 mm (L/D = 30), was used to measure the flow properties of TPS/C30B, PLA/C30B extruded materials and the hybrid blends. All tests were performed over a shear rate range of 50–3000 s^{-1}, at 165 °C with a prior melting time of 5 min. End corrections were not applied; thus, the viscosity values are reported as apparent viscosities. The setting of parameters and evaluation of raw data, as well as the Rabinowitsch's correction, were performed with the software LabRheo, provided with the equipment. The consistency index and the flow behavior index were obtained according to the power law model (Eqs. (2) and (3)).

$$\tau = K\dot{\gamma}^{n} \tag{2}$$

$$\eta = K\dot{\gamma}^{(n-1)} \tag{3}$$

where τ is the shear stress, $\dot{\gamma}$ is the shear rate at the capillary wall, η is the viscosity, K is the consistency index and n is the flow behavior index of the materials analyzed.

2.6. Thermogravimetric analysis

Thermogravimetric analyses were carried out for the extruded materials under nitrogen atmosphere on a TGA Q-500 equipment from TA Instruments (New Castle, USA). Approximately, 10 mg of sample were heated from 25 to 700 °C, at a 10 °C/min rate.

2.7. Phase morphology

The phase morphology of the samples was examined with a Jeol electron microscope, model JSM-6460LV (Akishima-shi, Japan), generally at the acceleration voltage of 20 kV. Samples were cryogenically fractured before observation. The fractured surfaces were vacuum-coated with gold before measurements. X-ray photoelectron spectroscopy (XPS) was used to analyze the cryofractured surfaces of injection-molded samples in a NORAN™ System 6 X-ray Microanalysis System, model C10015 (Thermo Fisher Scientific Inc., Middleton, WI, USA), linked to the Jeol electron microscope.

2.8. Tensile tests of extruded and compression-molded samples

Tensile tests were carried out at 21 °C in a Q-800 DMA equipment from TA Instruments (New Castle, DE, USA), according to the ISO 527-3 method, with extruded and compression-molded specimens with 13 ± 0.2 mm × 6 ± 0.2 mm × 0.8 ± 0.1 mm dimensions, conditioned at 21 °C, and 50% relative humidity, for a period of at least 48 h. The average value from a total of three measurements was taken. The samples were placed between a fixed and a moveable clamp, and the experiments were performed in tensile mode.

2.9. Injection molding

The pelletized samples were subsequently dried in an oven at 100 °C for 2 h. Samples for tensile tests were prepared in an injection-molding machine Arburg, model Allrounder 270S (Lossburg, Germany) to obtain specimens according to ASTM D638, type I (thickness 1.8 ± 0.1 mm). The five heating zones of the injection molding machine were maintained at 170, 180, 190 and 200 °C and 210 °C (from feed to die zone). The mold temperature was set at 30 °C. The injection and the back pressures were 90 MPa and 57 MPa, respectively. The injection speed was 6×10^{-5} m^3/s and the back time was 4 s. Before performing mechanical tests, the specimens were conditioned at 21 °C and 50% relative humidity for 48 h.

2.10. Tensile tests of extruded and injection-molded samples

Tensile tests were performed in a Instron Universal Testing Machine model 4204 (Norwood, MA, USA) equipped with a 1 kN load cell, at a speed of 1 mm/min. The average value from a total of seven measurements was taken. All data were recorded and processed by the software provided with the Instron equipment.

3. Results and discussion

A diffractometer with a high resolution at low angles was used to investigate C30B dispersion within TPS and PLA extruded materials. In Fig. 1(a–c) (trace I), the 0 0 1 reflection for the neat C30B was observed at $2\theta = 4.9°$, and revealed a d_{001} value of 1.8 nm. For TPS/C30B materials up to 5.0 mass% organoclay, no reflection was detected within the 0.9–10° (2θ) region (Fig. 1a). This result indicated that the 0 0 1 reflection of C30B was shifted to angles bellow 0.9° (2θ), with interlayer spacings higher than 9.8 nm. For the TPS samples with C30B at 7.5 and 10 mass% contents, broad reflections were observed around 4.5° and 4.3° (2θ), corresponding to d-values

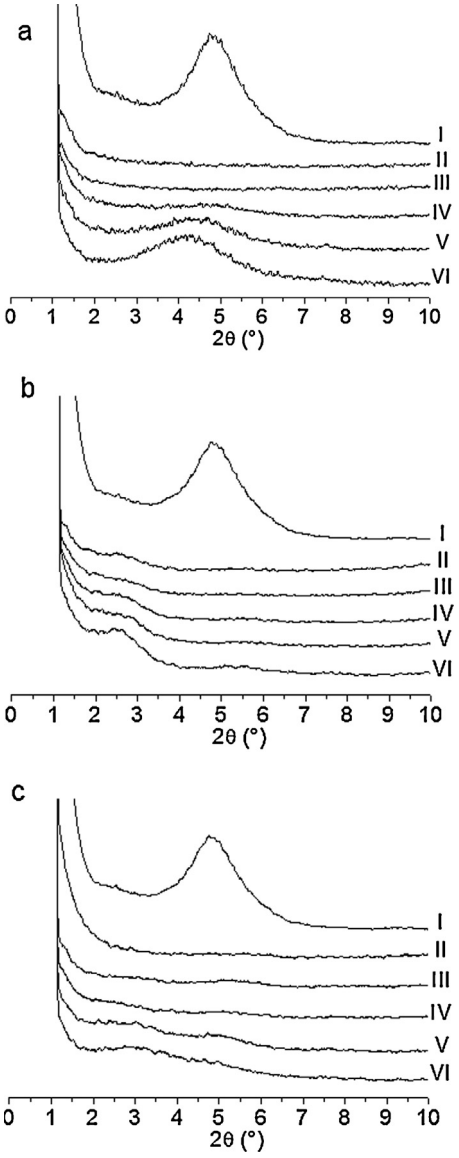

Fig. 1. X-ray diffractograms in the 2θ region of 0.6° to 10° for the neat C30B (traces I); (a) TPS, (b) PLA, (c) 70:30 TPS/PLA blend with the incorporation of C30B at 1.0 (traces II), 2.5 (traces III), 5.0 (traces IV), 7.5 (traces V), 10.0 (traces VI) mass%.

of approximately 2.0 nm. This result may be attributed to the presence of a fraction of C30B aggregates, in which starch molecules were partially intercalated. Although some authors reported on the incompatibility of hydrophilic thermoplastic starch with C30B (Chiou et al., 2006), the results of this work may be compared to those obtained by compounding potato starch with C30B in an internal mixer (Park, Lee, Park, Cho, & Ha, 2003). In this latter work, no reflection was found when C30B was incorporated at 2.5 mass% content, and a slight shift in the organoclay 0 0 1 reflection, from around 4.71° (2θ) to around 4.30° (2θ), was observed for the hybrids with 5 and 10 mass% C30B. The presence of two hydroxyethyl moieties in the intercalant of C30B explains its interaction with starch molecules. On the other hand, for all PLA/C30B materials (Fig. 1b), low-intensity reflections around 2.6° (2θ) were observed. The intensity of these reflections increased slightly with the increase in organoclay content, and indicated that the organoclay had interlayer spacings of approximately 3.4 nm, intercalated with PLA molecules. Similar results were obtained by other authors for PLA and C30B (Araújo, Botelho, Oliveira, & Machado, 2014; Duan, Thomas, & Huang, 2013; Fukushima, Tabuani, & Camino, 2012; Lai,

Table 1
Power law constants for glycerol-plasticized thermoplastic starch, poly(acid acid) and their blends, with or without the incorporation of the C30B.

Blend composition	K (Pa s)	n	R^2
TPS	10 399	0.27	0.998
TPS/C30B (1.0 mass%)	9727	0.31	0.999
TPS/C30B (2.5 mass%)	9332	0.36	0.999
TPS/C30B (5.0 mass%)	13 489	0.31	0.999
TPS/C30B (7.5 mass%)	21 281	0.28	0.998
TPS/C30B (10.0 mass%)	25 577	0.31	0.999
PLA (as received)	44 668	0.40	0.995
PLA (after extrusion)	964	0.32	0.996
PLA/C30B (1.0 mass%)	100 025	0.17	0.998
PLA/C30B (2.5 mass%)	51 286	0.25	0.995
PLA/C30B (5.0 mass%)	41 686	0.15	0.996
PLA/C30B (7.5 mass%)	125 892	−0.44	0.999
PLA/C30B (10.0 mass%)	25 150	−0.04	0.998
TPS/PLA	13 423	0.37	0.998
TPS/PLA/C30B (1.0 mass%)	25 118	0.29	0.997
TPS/PLA/C30B (2.5 mass%)	40 738	0.34	0.994
TPS/PLA/C30B (5.0 mass%)	81 234	0.28	0.999
TPS/PLA/C30B (7.5 mass%)	51 121	0.39	0.996
TPS/PLA/C30B (10.0 mass%)	21 579	0.60	0.998

Wu, Lin, & Don, 2014; Molinaro et al., 2013; Pluta, 2006; Zaidi et al., 2010), and attributed to hydrogen bonding interaction between the hydroxyethyl groups of the oraganoclay intercalant and carbonyl ester groups of PLA macromolecules. Anyway, the difference between PLA and TPS intercalation might be ascribed to the bulky ring structure of TPS, because in both cases hydrogen bonding interactions are favored.

It would be worth observing the diffractograms obtained for the TPS/PLA/C30B materials. In Fig. 1c (traces II–IV), following the results for TPS/C30B, no reflection was observed in the diffractograms for TPS/PLA hybrids with 1.0, 2.5 and 5.0 mass% C30B, which indicated that the 0 0 1 reflection of C30B was shifted to angles bellow 0.9° (2θ), with interlayer spacings higher than 9.8 nm. For the hybrids with 7.5 and 10.0 mass% C30B, shallow reflections around 3° and 4.5–5° (2θ) were envisaged. In this case, the reflection around 3° (2θ) was attributed to C30B layers intercalated with starch molecules, and the other broader and less intense reflection at 4.5–5° (2θ) was attributed to a very small amount of C30B aggregates. Anyway, these diffractograms corroborated the good affinity of C30B towards both TPS and PLA phases, and suggested an even better dispersion of the organoclay in the extruded blends in relation to TPS or PLA alone.

The melt flow characteristics of all extruded materials considered in this work were investigated by capillary rheometry at 165 °C, and the resulting curves are shown in Fig. 2(a–c), as apparent viscosity *versus* shear rate. Shear thinning behavior was observed for all samples. Comparing TPS and PLA alone, the virgin PLA presented higher viscosity values, but a less pronounced shear thinning behavior compared to TPS, as indicated by the higher flow index (n) value, shown in Table 1. However, for the extruded PLA sample, a severe reduction of viscosity was observed. In general, processing of PLA is preceded by humidity elimination, but even when this procedure was followed, degradation was observed (Souza et al., 2013). Viscosity reduction of PLA was attributed to both hydrolysis reaction and thermal degradation (Speranza, De Meo, & Pantani, 2014). Since the objective of the extrusion processing was to produce TPS/PLA hybrid blends, in which all components are hygroscopic, drying seemed an unrealistic procedure.

For TPS/C30B materials (Fig. 2a), the increase in organoclay content, from 1.0 to 10 mass% content, led to almost a half-decade increase of apparent viscosity, and indicated that both exfoliated (at a low C30B content), and particularly intercalated organoclay contributed positively to viscosity. For these materials, the flow index n (Table 1) showed typical values, within the range (0.27–0.56)

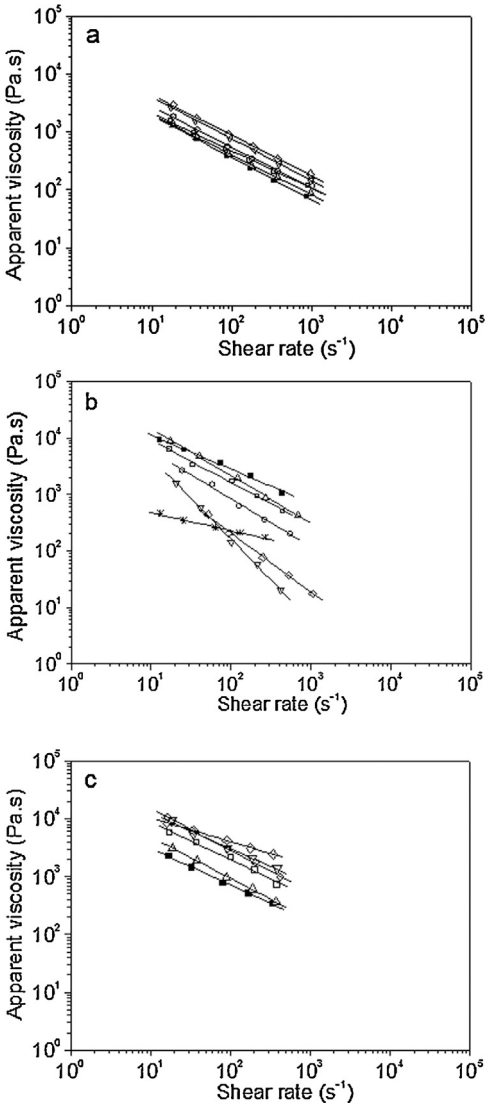

Fig. 2. Variation of apparent viscosity as a function of shear rate at 165 °C for (a) TPS alone (■) and hybrids, (b) PLA alone (■) and hybrids, and (c) neat 70:30 TPS/PLA blend (■) and hybrids, with the incorporation of C30B at 1.0 (△), 2.5 (□), 5.0 (○), 7.5 (▽), and 10.0 (◇) mass%.

previously reported for cornstarch submitted to thermomechanical treatments at different moisture contents (Vergnes & Villemaire, 1987). On the other hand, a substantial reduction of viscosity and n values was observed for PLA/C30B materials with increasing organoclay content (Fig. 2b, Table 1). Recently, the thermal decomposition process of a similar system composed of PLA and C30B at 0.5 and 2.5 mass% content was reported, and the nanocomposites were found more stable than PLA alone (Carrasco, Pérez-Maqueda, Santana, & Maspoch, 2014). In the last case, a dehumidifier was used prior to extrusion. When comparing the two hybrids, the authors observed that the incorporation of 2.5 mass% C30B to PLA led to a less thermally stable sample, attributed to the presence of C30B aggregates. In this study, the diffractograms of Fig. 1b revealed that the extrusion conditions led to intercalated C30B hybrids. Thus, the reduction of viscosity, mainly at 7.5 and 10.0 mass% C30B contents, and at high shear rates, might be indicating hydrolytic degradation to such an extent that topological constraints were extensively minimized.

Viscosity curves were also obtained for the 70:30 TPS/PLA blends, with or without the addition of C30B (Fig. 2c, Table 1). As

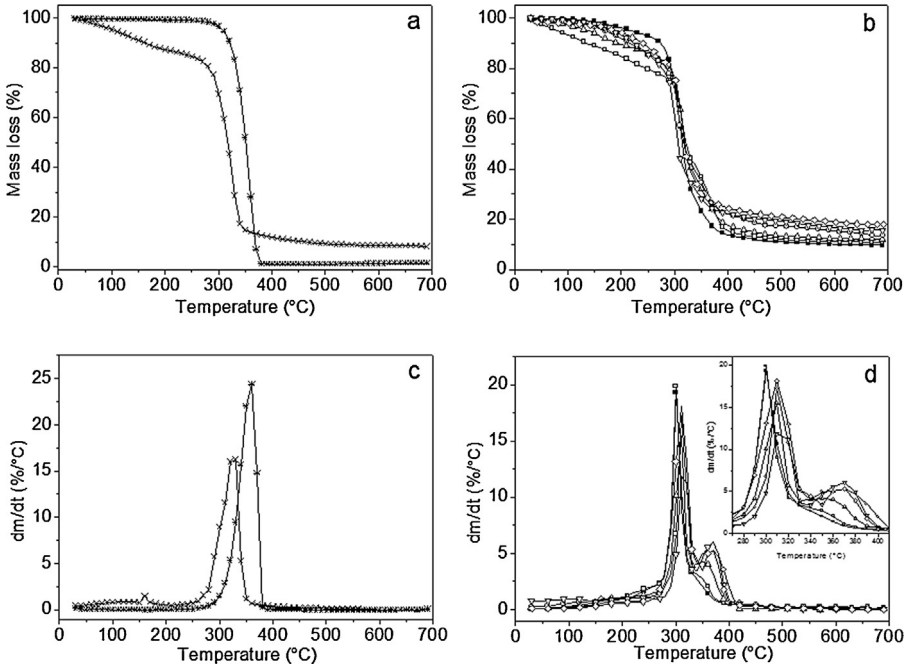

Fig. 3. TGA curves for (a) TPS (×) and PLA (□), and (b) neat 70:30 TPS/PLA blend (■) and hybrids, (c) DTG curves for TPS (×) and PLA (□), and (d) neat 70:30 TPS/PLA blend (■) and hybrids with the incorporation of C30B at 1.0% (□), 2.5% (△), 5.0 (○) 7.5% (▽), and 10.0 (◇) mass%.

expected, the melt viscosity for the neat TPS/PLA blend resulted in intermediary values between those determined for TPS and PLA, and the incorporation of C30B contributed to increase the blends viscosity. The flow index values seemed to be governed by the properties of TPS, the component added at a larger composition. However, no clear trend was followed by the consistency index K. It might be inferred that the more pronounced Newtonian character of the TPS/PLA hybrid with C30B at 10.0 mass% content (Table 1) would worsen conditions for further processing, such as injection molding.

The thermal stability of TPS, PLA, and TPS/PLA blends with and without the addition of C30B was evaluated by thermogravimetric analysis (TGA) under nitrogen atmosphere. The TGA curves are shown in Fig. 3(a and b). Up to 100 °C, mass loss is mainly attributed to humidity loss. From 100 °C to decomposition temperature, the mass loss observed for TPS and TPS/PLA/C30B at 1.0 mass% might be attributed to glycerol evaporation. With increasing organoclay content, a reduction of plasticizer loss was observed. The neat TPS/PLA blend showed the lowest onset degradation temperature (T_o = 284 °C), whereas TPS (T_o = 297 °C) and PLA (T_o = 332 °C) had higher thermal stabilities. For the hybrid blends, T_o decreased moderately, from 303 °C to 288 °C, as the C30B content was increased.

It is worth observing in Fig. 3(c and d) (DTG curves) that the maximum degradation rate was reached for PLA at T_{max} = 361 °C, and for TPS at T_{max} = 327 °C. While a single peak at T_{max} = 301 °C was observed for the neat TPS/PLA blend, two peaks were observed for the hybrid samples. The first peak, attributed to the maximum degradation rate of the TPS phase, varied from T_{max} = 302 °C to T_{max} = 313 °C with increasing C30B content. Lower T_{max} values for TPS/calcium montmorillonite hybrids in relation to TPS were previously observed, and were attributed to the catalytic effect of acidic sites of montmorillonite on the thermal degradation of the starch matrix (Magalhães & Andrade, 2010). Similar result was also observed for other hybrid systems (Ramos Filho, Mélo, Rabello, & Silva, 2005). The second peak, attributed to the maximum degradation rate of the PLA phase, varied from T_{max} = 357 °C to T_{max} = 369 °C with increasing C30B content. This result is in accordance with some authors, to whom the preparation of nanocomposites by adding organo-modified montmorillonites should be considered as a promising method to reduce PLA thermal degradation (Carrasco et al., 2014). In relation to PLA, other authors observed a slight increase in T_{max} for the PLA/C30B nanocomposites at 1.0, 3.0 and 5.0 phr organoclay content (Lai et al., 2014).

In this case, the TGA data also corroborated viscosity results for the TPS/PLA/C30B hybrids (Fig. 2), which suggested the protecting action of TPS against PLA degradation. More important, DTG curves gave additional evidence on the location of clay mineral particles in both TPS and PLA phases, as suggested by XRD results (Fig. 1). Also, as observed by some authors (Lai et al., 2014), the nucleating effect of the organoclay particles should not be neglected. XRD data in the 2θ region of 2° to 35° revealed PLA characteristic reflections with increasing intensities, as the content of C30B was increased (Fig. S1, Supplementary data).

As in most polymer blends, TPS and PLA are immiscible. Melt blending was performed without the addition of an organic compatibilizer and, as expected, the image of Fig. 4a, obtained for the neat TPS/PLA blend, shows a coarse morphology. Immiscibility was evidenced by the size, and the lack of adhesion between the two phases. For the extruded and compression-molded TPS/PLA/C30B materials in Fig. 4(b–f), the micrographs revealed that, as the organoclay content was increased from 2.5 to 10 mass%, at 10 mass% the PLA dispersed phase became undistinguished from the TPS matrix. This result was related to the role of the organoclay in the improvement of the system morphology. Considering that the organoclay interacted similarly with both components, and considering the viscosity results obtained, a rough estimation of viscosity ratios might be envisaged for the 70:30 TPS/PLA blends with added C30B. With increasing C30B contents, the viscosity ratio p and the capillary number might be expected to decrease, and p might approach the value p = 1. Contrarily to the morphology improvement, previously reported for C30B nanocomposites of TPS and poly(3-hydroxybutyrate-*co*-3-hydroxyvalerate) (PHBV) (Magalhães, Dahmouche, Lopes, & Andrade, 2013), no clear visualization of size reduction of the PLA dispersed phase was observed,

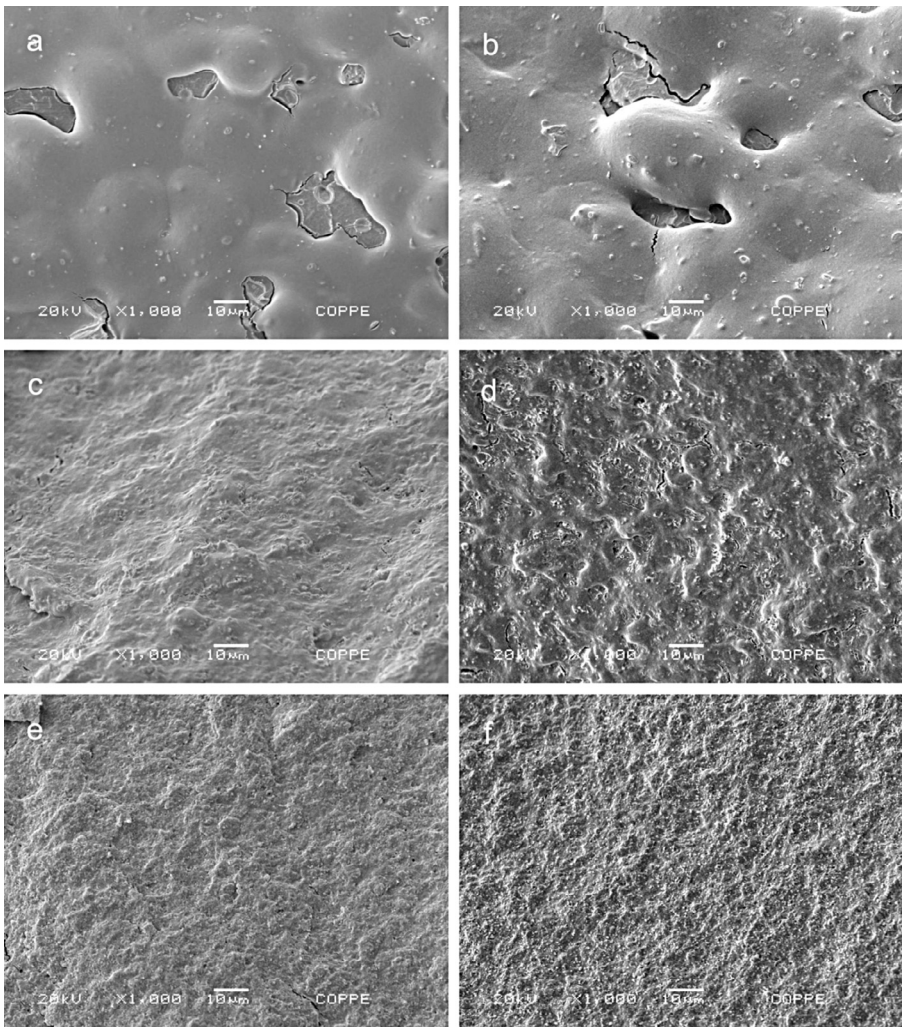

Fig. 4. SEM images for the extruded samples; neat 70:30 TPS/PLA blend (a), and for the hybrids with the incorporation of C30B at 1.0 (b), 2.5 (c), 5.0 (d), 7.5 (e) and 10.0 (f) mass%.

as the content of C30B was increased from 2.5 to 10 mass%. Thus, no indication on the location of the organoclay nanoparticles at the interface between the components could be suggested. Also, it was claimed that clay mineral particles would be incorporated preferentially into the polymer with the lowest melting temperature (Fenouillot et al., 2009). In this case, TPS has a lower melting temperature than PLA. However, as shown in Fig. 2 for TPS/C30B and PLA/C30B hybrids, with increasing contents of the organoclay, while the viscosity of TPS was increased, the viscosity of PLA was decreased, and the melting pattern might be changed even during the extrusion step. As the viscosity of the polymeric components seems to interfere on the location of the clay minerals particles (Naderi, Lafleur, & Dubois, 2008), it might be presumed that C30B tended to be almost equally incorporated in both TPS and PLA phases during processing, and eventually at the interface, as its content was increased. However, it seems as if the amount of organoclay was not enough to saturate the interface between the TPS matrix and PLA droplets, probably because exfoliated organoclay layers or organoclay aggregates were preferentially located within both polymers.

The mechanical properties of the TPS/PLA hybrid blends were investigated by two methods, using compression-molded (Fig. 5) and injection-molded specimens (Fig. 6). These results were analyzed independently, since they were acquired by different methods. In Fig. 5a, for compression-molded samples, the rigid character of PLA, to which the elastic modulus was determined as $E = 3146.3 \pm 311.8$ MPa, and the soft nature of TPS were once more revealed. In Fig. 5b, even for the neat TPS/PLA blend, the elastic modulus (190.2 ± 18.1 MPa) increased in relation to TPS alone ($E = 82.3 \pm 7.9$ MPa). For the compression-molded hybrids, the moduli varied from $E = 167.5 \pm 14.8$ MPa to 501.4 ± 52.2 MPa, by incorporating 1.0 to 7.5 mass% C30B. This result was expected because of the rigid nature of the filler. However, a substantial decrease in tensile stress at break (σ_{max}) was observed for the neat TPS/PLA blend ($\sigma_{max} = 1.5 \pm 0.1$ MPa) and the C30B hybrids, in relation to TPS and PLA. For TPS, this value was $\sigma_{max} = 4.4 \pm 0.4$ MPa and, for PLA, $\sigma_{max} = 5.3 \pm 0.5$ MPa. For the TPS/PLA hybrids, σ_{max} varied from 1.7 ± 0.2 MPa for C30B incorporated at a 1.0 mass% content to $\sigma_{max} = 3.4 \pm 0.4$ MPa for the hybrid with C30B at a 7.5 mass% content. As for the elongation at break, ε_{max}, their values varied for the same hybrids, respectively, from $0.8 \pm 0.1\%$ to $1.3 \pm 0.01\%$, in relation to $\varepsilon_{max} = 15.2 \pm 1.1\%$ for TPS.

For the hybrid prepared with C30B at 10.0 mass% content, the E and σ_{max} values decreased to $E = 383.5 \pm 41.2$ MPa and $\sigma_{max} = 2.9 \pm 0.3$ MPa, respectively. This result was not expected, as long as increasing values were obtained with increasing contents of C30B. However, the plasticizing effect of the C30B intercalant, also incorporated at a higher amount, might have contributed to the less rigid character of this hybrid, for which ε_{max} reached $1.9 \pm 0.01\%$.

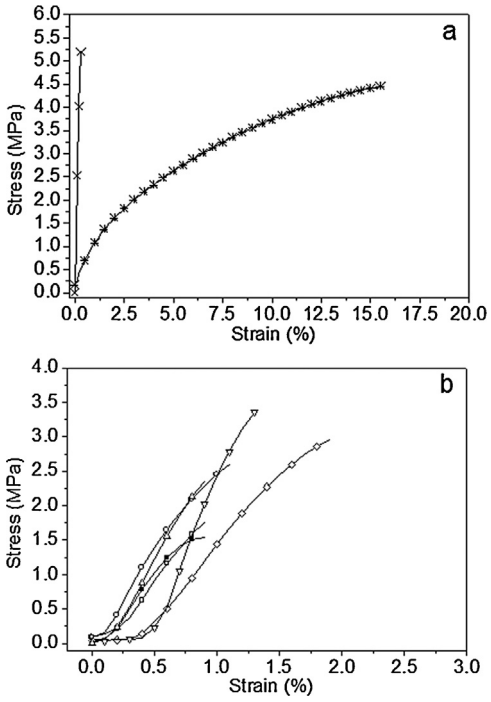

Fig. 5. Stress *versus* strain curves for the extruded samples; (a) TPS (□) and PLA (×); (b) neat 70:30 TPS/PLA blend (■) and hybrids with the incorporation of C30B at 1.0% (□), 2.5% (△), 5.0 (○) 7.5% (▽), and 10.0 (◇) mass%.

It is worth noting that the relatively better results of tensile tests (in relation to the neat TPS/PLA blend) for the hybrids, to which C30B was incorporated at 5.0 to 10.0 mass% contents, followed the previously rough estimation for viscosity ratios. Because of this result, these extruded samples as well as the neat 70:30 TPS/PLA blend were chosen to be submitted to injection molding, to investigate possible changes of morphology and mechanical properties.

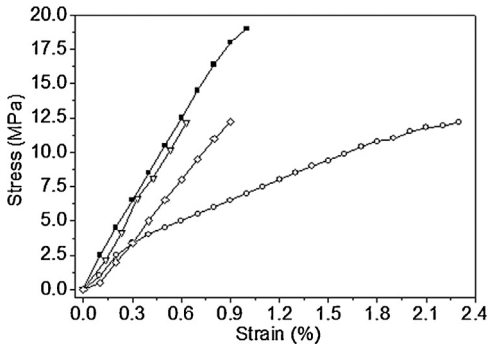

Fig. 6. Stress *versus* strain curves for the injection-molded samples; neat 70:30 TPS/PLA blend (■) and for the hybrids the incorporation of C30B at 5.0 (○) 7.5% (▽), and 10.0 (◇) mass%.

The mechanical properties of the injection-molded samples were evaluated (Fig. 6). The highest stress at break (σ_{max} = 18.9 MPa) was obtained for the neat TPS/PLA blend. Differently from the previous result obtained for the compression-molded sample, the injection-molded hybrid with 10.0 mass% C30B did not show the highest ductibility. The highest elastic modulus (E = 11.4 ± 3.8 MPa) and lowest elongation at break (ε_{max} = 0.55 ± 0.16%) were determined for the hybrid with 7.5 mass% C30B.

The best ductibility was achieved for the TPS/PLA/C30B hybrid with 5.0 mass% organoclay (E = 1091.5 ± 181.3 MPa, σ_{max} = 11.2 ± 2.2 MPa, ε_{max} = 2.33 ± 1.4%). Bearing in mind XRD results, the incorporation of 5.0 mass% C30B led to a higher degree of exfoliation, which certainly contributed to the better fluidity during injection molding and the highest ductibility. Moreover, the more pronounced Newtonian character of the TPS/PLA hybrid with C30B at 10.0 mass%, as shown before (Table 1), indeed made injection molding more difficult.

To verify the effect of injection molding on morphology, cryofractured surfaces of the injection-molded samples were analyzed by SEM (Fig. 7). Although more sensitive to the electron beam, the

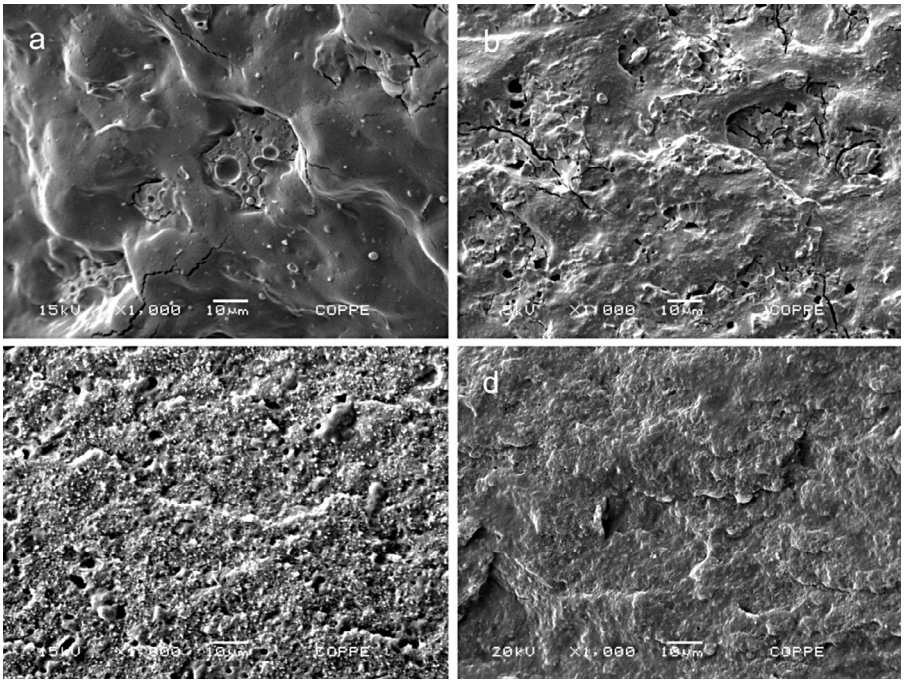

Fig. 7. SEM images for the injection-molded samples; neat 70:30 TPS/PLA blend (a), and for the hybrids the incorporation of C30B at 5.0 (b) 7.5% (c), and 10.0 (d) mass%.

neat TPS/PLA blend in Fig. 7a showed a similar image to that taken for the compression-molded sample (Fig. 4a). The SEM images for the hybrids with 5.0 and 7.5 mass% C30B in Fig. 7(b and c) were characterized by the appearance of microvoids much larger in diameter than those observed for the corresponding compression-molded samples. The appearance of these microvoids might be related to the loss of some droplets of PLA dispersed phase during cryofracturing. If this supposition were true, it indicated a very small amount of C30B at the interface. No particular feature seems to distinguish the image observed for the injection-molded hybrid with C30B at 10 mass% content from that obtained for the compression-molded sample with the same content of the filler. This result might be probably related to a higher amount of the organoclay at the interface.

Using XPS to analyze the cryofractured surfaces of injection-molded samples, the results revealed widespread distribution of Mg, Al and Si (Supplementary data, Figs. S2–S4), according to the previous supposition on incorporation of C30B within both components phases.

4. Conclusions

The favorable interaction between the organoclay intercalant and the molecules of both components, starch and PLA, suggested by XRD and TGA results, seemed to dictate the properties of extruded TPS/PLA/C30B hybrids. XRD data suggested no specific preference for one of the blend components. TGA indicated the stabilizing effect of C30B on the PLA phase, as the content of the organoclay increased. Shear viscosities, determined for each component in the presence of the same organoclay contents, roughly indicated the tendency for achieving a viscosity ratio around $p = 1$, as higher contents of organoclay were incorporated. For the extruded and compression-molded samples, the results of tensile tests followed this estimation. The SEM images revealed that the morphology, even after injection molding, remained the same for the TPS/PLA hybrid blend, prepared with C30B at the highest content (10.0 mass%). The high degree of organoclay dispersion, associated with the highest pseudoplasticity of the 5.0 mass% hybrid blend, and the structuring characteristic of the process, certainly contributed to the highest ductibility of this TPS/PLA hybrid material after processing by injection molding.

Acknowledgments

The authors acknowledge the Brazilian agencies Conselho Nacional de Desenvolvimento Científico e Tecnológico (CNPq) (Grant N° 307237/2011-7), Fundação de Amparo à Pesquisa do Estado do Rio de Janeiro (FAPERJ) (Grant N° E-26/102964/2011), and Coordenação para o Aperfeiçoamento de Pessoal de Nível Superior (CAPES) for financial support.

Appendix A. Supplementary data

Supplementary data associated with this article can be found, in the online version, at http://dx.doi.org/10.1016/j.carbpol.2014.10.018.

References

Araújo, A., Botelho, G., Oliveira, M., & Machado, A. V. (2014). Influence of clay organic modifier on the thermal-stability of PLA based nanocomposites. *Applied Clay Science*, *88–89*, 144–150.

Arroyo, O. H., Huneault, M. A., Favis, B. D., & Bureau, M. N. (2010). Processing and properties of PLA/thermoplastic starch/montmorillonite nanocomposites. *Polymer Composites*, *31*, 114–127.

Ayana, B., Suin, S., & Khatua, B. B. (2014). Highly exfoliated eco-friendly thermoplastic starch (TPS)/poly(lactic acid)(PLA)/clay nanocomposites using unmodified nanoclay. *Carbohydrate Polymers*, *110*, 430–439.

Carrasco, F., Pérez-Maqueda, L. A., Santana, O. O., & Maspoch, M. Ll. (2014). Enhanced general analytical equation for the kinetics of the thermal degradation of poly(lactic acid)/montmorillonite nanocomposites driven by random scission. *Polymer Degradation and Stability*, *101*, 52–59.

Chiou, B.-S., Yee, E., Wood, D., Shey, J., Glenn, G., & Orts, W. (2006). Effects of processing conditions on nanoclay dispersion in starch-clay nanocomposites. *Cereal Chemistry*, *83*, 300–305.

Duan, Z., Thomas, N. L., & Huang, W. (2013). Water vapour permeability of poly(lactic acid) nanocomposites. *Journal of Membrane Science*, *445*, 112–118.

Feng, J., Chan, C. M., & Li, J. X. (2003). A method to control the dispersion of carbon black in an immiscible polymer blend. *Polymer Engineering and Science*, *43*, 1058–1063.

Fenouillot, F., Cassagnau, P., & Majesté, J.-C. (2009). Uneven distribution of nanoparticles in immiscible fluids: morphology development in polymer blends. *Polymer*, *50*, 1333–1350.

Fukushima, K., Tabuani, D., & Camino, G. (2012). Poly(lactic acid)/clay nanocomposites: effect of nature and content of clay on morphology, thermal and thermo-mechanical properties. *Materials Science and Engineering C*, *32*, 1790–1795.

Horozov, T. S. (2008). Foams and foam films stabilised by solid particles. *Current Opinion in Colloid & Interface Science*, *13*, 134–140.

Huneault, M. A., & Li, H. (2007). Morphology and properties of compatibilized polylactide/thermoplastic starch blends. *Polymer*, *48*, 270–280.

Hunter, T. N., Pugh, R. J., Franks, G. V., & Jameson, G. J. (2008). The role of particles in stabilising foams and emulsions. *Advances in Colloid and Interface Science*, *137*, 57–81.

Lai, S.-M., Wu, S.-H., Lin, G.-G, & Don, T.-M. (2014). Unusual mechanical properties of melt-blended poly(lactic acid) (PLA)/clay nanocomposites. *European Polymer Journal*, *52*, 193–206.

Luckachan, G. E., & Pillai, C. K. S. (2011). Biodegradable polymers—A review on recent trends and emerging perspectives. *Journal of Polymers and the Environment*, *19*, 637–676.

Magalhães, N. F., & Andrade, C. T. (2010). Calcium bentonite as reinforcing nanofiller for thermoplastic starch. *Journal of the Brazilian Chemical Society*, *21*, 202–208.

Magalhães, N. F., Dahmouche, K., Lopes, G. K., & Andrade, C. T. (2013). Using an organically-modified montmorillonite to compatibilize a biodegradable blend. *Applied Clay Science*, *72*, 1–8.

Molinaro, S., Romero, M. C., Boaro, M., Sensidoni, A., Lagazio, C., Morris, M., et al. (2013). Effect of nanoclay-type and PLA optical purity on the characteristics of PLA-based nanocomposite films. *Journal of Food Engineering*, *117*, 113–123.

Naderi, G., Lafleur, P. G., & Dubois, C. (2008). The influence of matrix viscosity and composition on the morphology, rheology, and mechanical properties of thermoplastic elastomer nanocomposites based on EPDM/PP. *Polymer Composites*, *29*, 1301–1309.

Park, H.-M., Lee, W., Park, C.-Y., Cho, W.-J., & Ha, C.-S. (2003). Environmentally friendly hybrids. Part I Mechanical, thermal, and barrier properties of thermoplastic starch/clay nanocomposites. *Journal of Materials Science*, *38*, 909–915.

Pluta, M. (2006). Melt compounding of polylactide/organoclay: Structure and properties of nanocomposites. *Journal of Polymer Science, B: Polymer Physics*, *44*, 3392–3405.

Ramos Filho, F. G., Mélo, T. J. A., Rabello, M. S., & Silva, S. M. L. (2005). Thermal stability of nanocomposites based on polypropylene and bentonite. *Polymer Degradation and Stability*, *89*, 383–392.

Schwach, E., Six, J.-L., & Avérous, L. (2008). Biodegradable blends based on starch and poly(lactic acid): Comparison of different strategies and estimate of compatibilization. *Journal of Polymers and the Environment*, *16*, 286–297.

Souza, D. H. S., Dahmouche, K., Andrade, C. T., & Dias, M. L. (2013). Synthetic organofluoromica/poly(lactic acid) nanocomposites: Structure, rheological and thermal properties. *Applied Clay Science*, *80–81*, 259–266.

Speranza, V., De Meo, A., & Pantani, R. (2014). Thermal and hydrolytic kinetics of PLA in the molten state. *Polymer Degradation and Stability*, *100*, 37–41.

Sundararaj, U., & Macosko, C. W. C. W. (1995). Drop breakup and coalescence in polymer blends: the effects of concentration and compatibilization. *Macromolecules*, *28*, 2647–2657.

Vergnes, B., & Villemaire, J. P. (1987). Rheological behaviour of low moisture molten maize starch. *Rheological Acta*, *26*, 570–576.

Wang, N., Yu, J., & Ma, X. (2007). Preparation and characterization of thermoplastic starch/PLA blends by one-step reactive extrusion. *Polymer International*, *56*, 1440–1447.

Wu, S. (1987). Formation of dispersed phase in incompatible polymer: Interfacial and rheological effects. *Polymer Engineering and Science*, *27*, 335–343.

Zaidi, L., Bruzaud, S., Bourmaud, A., Médéric, P., Kaci, M., & Grohens, Y. (2010). *Journal of Applied Polymer Science*, *116*, 1357–1365.

Zhang, J. F., & Sun, X. (2004). Mechanical properties of poly(lactic acid)/starch composites compatibilized by maleic anhydride. *Biomacromolecules*, *5*, 1446–1451.